Journal of Solid State Chemistry **160,** 460–468 (2001)
doi:10.1006/jssc.2001.9274, available online at http://www.idealibrary.com on IDEAL®

Solid State NMR, X-Ray Diffraction, and Infrared Characterization of Local Structure in Heat-Treated Oxyhydroxyapatite Microcrystals: An Analog of the Thermal Decomposition of Hydroxyapatite during Plasma-Spray Procedure

P. Hartmann[1] and C. Jäger

Institut für Optik und Quantenelektronik, Friedrich-Schiller-Universität Jena, Max-Wien-Platz 1, D-07743 Jena, Germany

St. Barth

Hermsdorfer Institut für Technische Keramik Marie-Curie Str. 17, D-07629 Hermsdorf, Germany

J. Vogel

Otto-Schott-Institut, Friedrich-Schiller-Universität Jena, Fraunhoferstraße 6, D-07743 Jena, Germany

and

K. Meyer

Institut für Physikalische Chemie, Friedrich-Schiller-Universität Jena, Lessingstr. 10, D-07743 Jena, Germany

Received December 16, 2000; in revised form May 30, 2001; accepted June 8, 2001

The structure of plasma-sprayed hydroxyapatites possesses a variety of partially dehydrated hydroxyapatite structures. Nuclear magnetic resonance, IR spectroscopy, and X-ray diffraction have been used to analyze the structure of partially dehydrated hydroxyapatites. The oxyhydroxyapatites are prepared from crystalline hydroxyapatite by thermal treatment in air. The obtained results enable an advanced phase analysis of plasma-sprayed hydroxyapatite layers. © 2001 Academic Press

Key Words: **hydroxyapatite; solid state nuclear magnetic resonance; IR spectroscopy.**

INTRODUCTION

Plasma-sprayed hydroxyapatite coatings are important today as biomineral analogs. A drawback of this coating technique is the extremely high temperature of the plasma used leading to partial thermal decomposition and dehydration of the hydroxyapatite.

The aim of the present investigations is the experimental simulation of the dehydration and further decomposition of hydroxyapatite during the plasma spraying procedure. During plasma spraying hydroxyapatite particles of about 50 microns are heated to about 10,000°C for some milliseconds. The overall thermal energy deposit is comparable to that of a long time heat treatment at significantly lower temperatures. Therefore, long time heat treatment at temperatures below 1300°C has been used to simulate the course of the decomposition and dehydration of hydroxyapatite during the plasma spraying. As is well known, at nearly 900°C, hydroxyapatite starts to decompose by evaporating water and forming partially or completely dehydrated oxyhydroxyapatite (1, 2, 12):

$$Ca_{10}(PO_4)_6(OH)_2 \rightarrow Ca_{10}(PO_4)_6(OH)_{2-2x}O_x + xH_2O,$$
$$\text{with } 0 \le x \le 1. \qquad [1]$$

For x values below about 0.5 the channel structure of the apatite remains almost unchanged. If x reaches a critical value (typically at temperatures above 1200°C) the destruction of the apatite channel structure occurs, and an equilibrium with tricalcium phosphate (TCP, $Ca_3(PO_4)_2$) and tetracalcium phosphate (TeCP, $Ca_4(PO_4)_2O$) exists:

$$Ca_{10}(PO_4)_6O \rightarrow Ca_4(PO_4)_2O + 2Ca_3(PO_4)_2 \qquad [2]$$
$$\text{oxyapatite} \qquad \text{TeCP} \qquad \text{TCP}$$

[1]To whom correspondence should be addressed.

0022-4596/01 $35.00

Finally, TCP melts at 1730°C, whereas TeCP melts incongruently at 1630°C leaving CaO as a residual solid. It should be noted that equilibrium is not obtained during the plasma spraying procedure. Rather than well-defined crystalline phases, the high temperatures and the huge cooling rates result in various intermediate states of the final coatings. Investigations on commercial plasma-sprayed hydroxyapatites possess at most only small amounts of TCP or TeCP. The major phases of the plasma-sprayed coating are X-ray amorphous partially dehydrated calcium monophosphate structures (3). Sfihi *et al.* (12) suggest that plasma-sprayed hydroxyapatite coating on prothesis could contain more than 70% of oxyapatite.

Obviously, the structure and therefore the biological properties of plasma-sprayed hydroxyapatite are not identical to those of the initial crystalline hydroxyapatite. The influence of the structural changes on the properties of the final coating is not completely known. However, it is well known that reaction products with significantly higher solubility, compared with that of crystalline hydroxyapatite, results in decreased biological long-term stability of the plasma-sprayed coatings. In the present study we combine solid state nuclear magnetic resonance (NMR), IR spectroscopy, and X-ray diffraction to analyze the structure of partially dehydrated oxyhydroxyapatites and compare it with that of plasma-sprayed hydroxyapatite.

EXPERIMENTAL

The initial hydroxyapatite powder (particle size 40 μm–100 μm) was highly crystalline and stoichiometric. It is identically to that used for the commercial production (FRIADEM GmbH, Germany) of human teeth root implants (3, 4). It was produced in analogy to the procedure described in Ref. (4). To keep the investigations comparable to the plasma spray procedure the apatites were heat-treated in air using an electrically heated furnace, in contrast to the method of Refs. (5, 12). As an important consequence of the "in air" heat treatment, hydroxyapatites can absorb atmospheric water during cooling. Thermal treatment was realized in two series. Series A has been heat-treated at a fixed temperature of 1100°C for variable times and series B at different temperatures for a fixed time of 2 h. Table 1 shows the thermal history of the investigated samples. X-ray powder patterns were collected using a SIEMENS diffractometer D 5000 (40 kV, 30 mA, scanning rate 0.02 deg/s, CuKα radiation). For the exposure of the NMR spectra a BRUKER AMX 400 and a TECMAG (300 MHz) spectrometer were used. The one-dimensional ^{1}H and ^{31}P spectra were obtained using magic angle spinning (MAS) with rotation rates up to $\omega_{max}/2\pi = 30$ kHz, typical $\pi/2$ pulse length of $t_w = 2$ μs–5 μs, and repetition rates of 200 s. The chemical shifts are referred to a solution of phosphoric acid (85%) for ^{31}P and tetramethylsilane for ^{1}H. The two-dimensional (2D) double-quantum NMR spectra (^{1}H, ^{31}P) were obtained using the BABA pulse sequence (6) using excitation and reconversion periods of 640 μs. The 256×64 data points were collected rotor-synchronized, according to the States method, and with typically 256 scans per increment. The ^{1}H–^{31}P 2D HETeroCORrelation spectra (HETCOR) are obtained using cross polarization (7) with variable magnitude of the ^{31}P contact pulse (contact time $t_{cp} = 5$ ms). The IR spectra were measured in the mid-IR region between 4000 and 400 cm^{-1} with a resolution of 4 cm^{-1} using a BRUKER IFS 66 FT-IR spectrometer. The samples were prepared by grinding with Nujol to avoid the adsorption of atmospheric water vapor. The ratio between the amounts of the sample and Nujol was determined by weighing. The absorbance spectra were recorded from the mixtures of the samples with Nujol which were applied to an IR window with an undefined thickness. The absorbance spectrum of pure Nujol with an unknown thickness was measured as reference. The Nujol spectrum weighted with a thickness factor for the compensation of the bands of the C–H deformation vibrations was subtracted from the absorbance spectra of the samples. For the evaluation of the intensity of the O–H stretching band the absorbance spectra of the samples were scaled to a constant sample–Nujol ratio of 0.5 and to the unknown thickness of the reference sample Nujol by means of the thickness factor. This kind of scaling allows a semi-quantitative characterization of the loss of O–H groups with an estimated error of about $\pm$ 5%. The intensity of the band of the O–H stretching vibrations was determined as integral intensity between 3590 and 3533 cm^{-1} after a linear baseline correction between these limits.

TABLE 1
Thermal History of the Investigated Hydroxyapatite Samples

Sample	Temperature (°C)	Time (h)
A1	1100	0.5
A2	1100	1
A3	1100	2
A4	1100	4
A5	1100	8
A6	1100	16
B1	1000	2
B2	1050	2
B3	1100	2
B4	1150	2
B5	1200	2
B6	1250	2
B7	1280	2

RESULTS AND DISCUSSION

Plasma-Sprayed Hydroxyapatite

As is known from the literature (3), the XRD patterns of crystalline hydroxyapatite and plasma-sprayed hy-

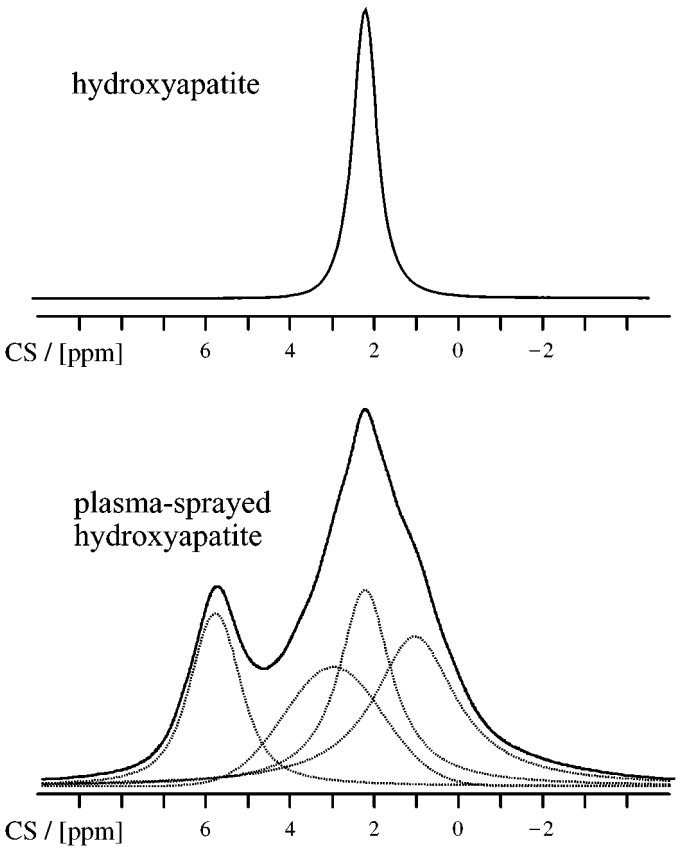

FIG. 1. ^{31}P MAS NMR spectra and fit simulation of crystalline hydroxyapatite and plasma-sprayed hydroxyapatite (resonance frequency $\nu_0 = 161.92$ MHz; spinning speed $\nu_R/2\pi = 12.5$ kHz, and repetition time $t_{re} = 200$ s.) The line fit (dotted lines) indicates several different nonequivalent phosphorus positions in the structure of the plasma-sprayed hydroxyapatite.

droxyapatite are very similar except for significant intensity differences. The XRD characterization of changes induced by the plasma spraying procedure is complicated due to the formation of amorphous phases. Amorphous phases produce a structured diffuse X-ray background which is hard to analyze. In most cases the only crystalline phase observed is HA. This was often interpreted as implying that the crystal structure of the initial HA is retained in the plasma-sprayed layer. In contrast, solid state NMR allows characterization of local atomic environments in both crystalline and amorphous phases. Figure 1 shows the ^{31}P and Fig. 2 the ^{1}H MAS NMR spectra of crystalline hydroxyapatite compared with those of plasma-sprayed hydroxyapatite. Both apatite NMR spectra show only a single line position at 2.3 ppm for ^{31}P and -0.09 ppm for ^{1}H, respectively. It should be noted that the MAS line width is a function of the degree of order. In other words the MAS line widths of different crystalline hydroxyapatites are slightly different depending on the preparation of the hydroxyapatite sample. In contrast, the spectra of the plasma-sprayed hydroxyapatite possess several additional line positions. The additional line positions prove significant structural changes during the plasma spraying procedure. However, the ^{31}P lines positions do not fit those of the crystalline calcium phosphates such as α-tricalcium phosphate (3, 5), β-tricalcium phosphate (3, 5), or tetracalcium phosphate (3). The thermal decomposition into those crystalline phosphates could therefore be excluded. Moreover, the observed variety and continuous variation of positions suggested that the plasma-sprayed layer consists of partially dehydrated oxyhydroxyapatite structures rather than well-defined stoichiometric phases.

Heat-Treated Oxyhydroxyapatites as Model Compounds for Plasma-Sprayed Hydroxyapatites

IR spectroscopy and NMR spectroscopy were used to characterize the structure of heat-treated hydroxyapatites.

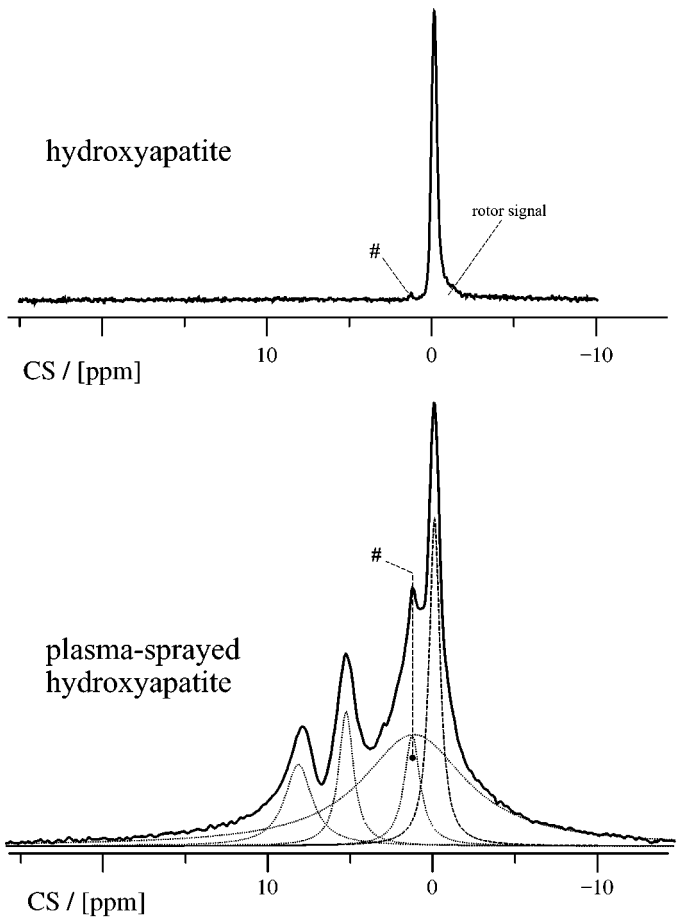

FIG. 2. ^{1}H MAS NMR spectra and fit simulation of crystalline hydroxyapatite and plasma-sprayed hydroxyapatite (resonance frequency $\nu_0 = 300.04$ MHz, spinning speed $\nu_R/2\pi = 12.5$ kHz, and $t_{re} = 5$ s). The line fit (dotted lines) indicates several different nonequivalent hydrogen positions in the structure of the plasma-sprayed hydroxyapatite. The marked rotor signals in the spectrum of crystalline HA are caused by protons of the MAS spinner. The line position marked by # represents physically adsorbed water.

Figure 3 shows the ^{31}P MAS NMR spectra of the hydroxyapatite samples heat-treated for a fixed time of 2 h at different temperatures (series B). Heat treatment of the apatite results in increasing line width of the typical apatite line at $\delta_{iso} = 2.3$ ppm, and splitting into four lines (A–D). That result is in contrast to the splitting in only two lines, as reported by Sfihi *et al.* (12) and McPherson *et al.* (13) for heat treatment under vacuum conditions.

2D correlation NMR showed that different phosphorus environments were intimately mixed in all samples, with no large-scale phase separation. As an example Fig. 4 shows the ^{31}P double-quantum spectrum of sample B7 (1280°C/2 h). The spectrum possesses a strong correlation peak between the phosphorus position D and positions A, B, and C. Hence, the phosphorus double-quantum spectrum is consistent with the hypothesis that all NMR line positions belong to only one dehydrated oxyhydroxyapatite single phase.

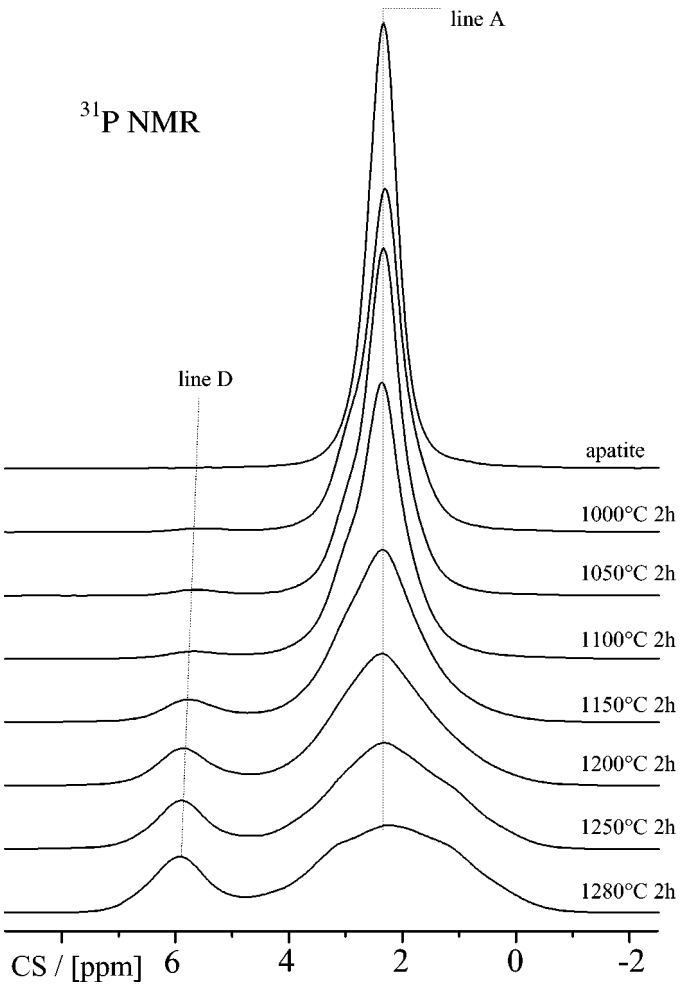

FIG. 3. ^{31}P MAS NMR spectra of the heat-treated hydroxyapatite samples of series B (fixed time of 2 h) compared to the initial crystalline hydroxyapatite (resonance frequency $\nu_0 = 161.92$ MHz, spinning speed $\nu_R/2\pi = 12.5$ kHz, and repetition time $t_{re} = 200$ s).

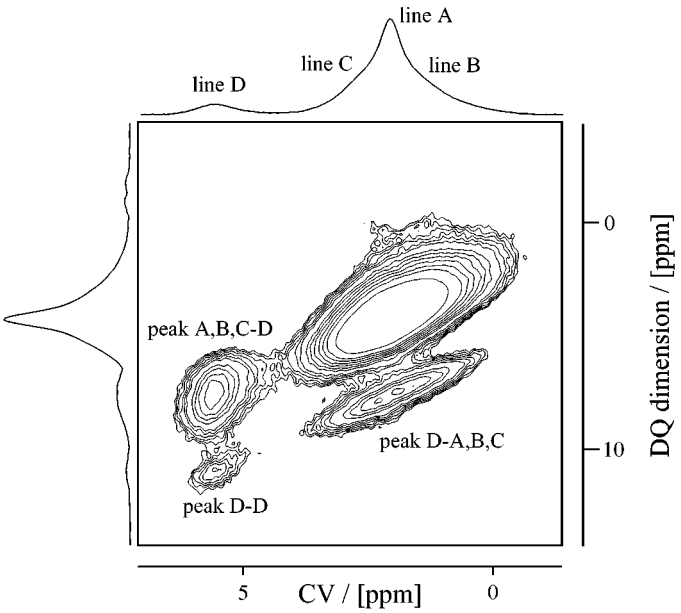

FIG. 4. 2D double-quantum correlation spectrum of sample B7 (1280°C/2 h). The resonance frequency was $\nu_0 = 161.92$ MHz, spinning frequency $\omega_R/2\pi = 12.5$ kHz, pulse width $t_w = 5$ μs, and repetition time $t_r = 200$ s. Both the double-quantum excitation and reconversion periods were 640 μs. The 256 × 64 data points were collectively rotor-synchronized, by the States method, and with 256 scans per point.

The relative content, the isotropic chemical shifts (δ_{iso}), and the MAS line width ($\nu_{1/2}$) of the four spectral components are drawn in Fig. 5 as a function of the temperature. The chemical shift and the MAS line width of line A are equal to those of crystalline hydroxyapatite and are, therefore, attributed to an almost perfect hydroxyapatite short-range structure in the samples B1–B4. The relative intensity of this line remains constant at about 25% of total until 1150°C. Between 1150°C and 1280°C the intensity decreases to 6% while the MAS line width simultaneously increases to about 1.0 ppm. The increasing line width suggests increasing disorder of the environment for these P atoms at temperatures above 1150°C (B5–B7).

The chemical shift of line B (starting at $\delta_{iso} = 2.4$ ppm) is close to that of line A. However, the line width (starting at $\nu_{1/2} = 1.2$ ppm) is significantly higher. The relative content of the corresponding phosphorus position decreases from about 80% in sample B1 (1000°C) to less than 35% in sample B4 (1150°C). Starting with sample B4 (1150°C), both the isotropic chemical shift (from 2.4 ppm to 1.5 ppm) and the MAS line width (from 1.2 ppm to 2.15 ppm) change significantly. The changes in line width as a function of the temperature are very similar for line A and line B. Furthermore, the intensities of both lines decrease simultaneously in the range between 1150°C and 1280°C.

In contrast to lines A and B, lines C and D increase in intensity with temperature, but their chemical shifts change

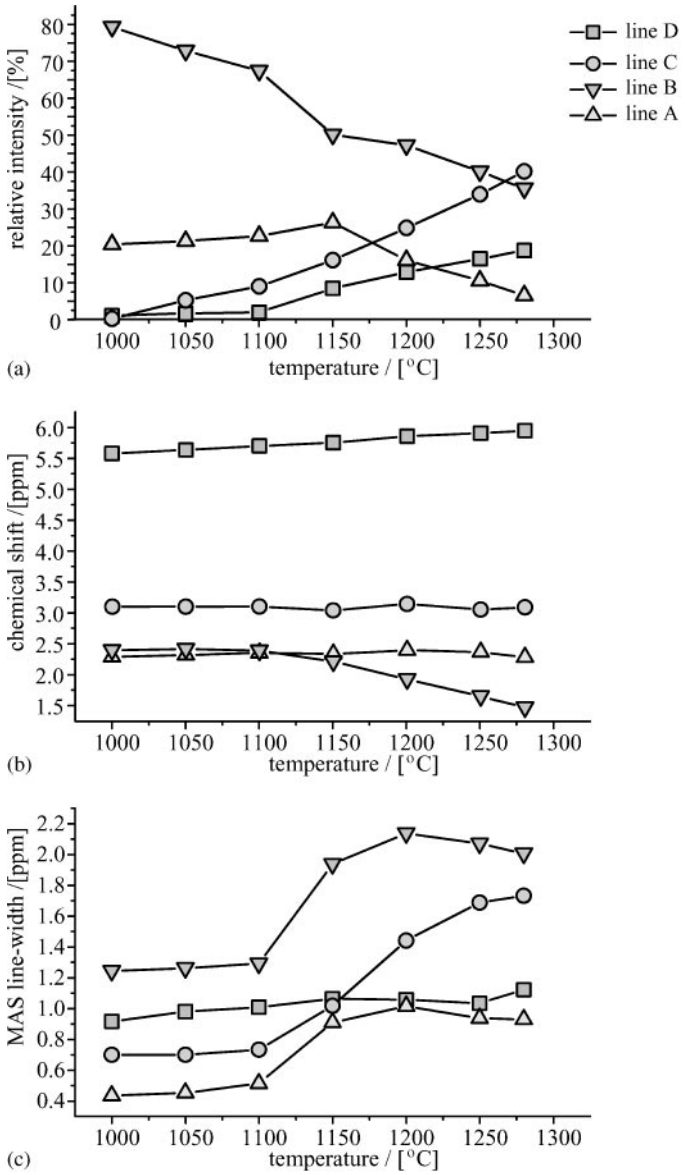

FIG. 5. Fit analysis of the ^{31}P NMR spectra of the heat-treated hydroxyapatites of series B. (a) Relative phosphorus content of the four different lines; (b) isotropic chemical shifts δ_{iso}; (c) MAS line width at half intensity $\nu_{1/2}$.

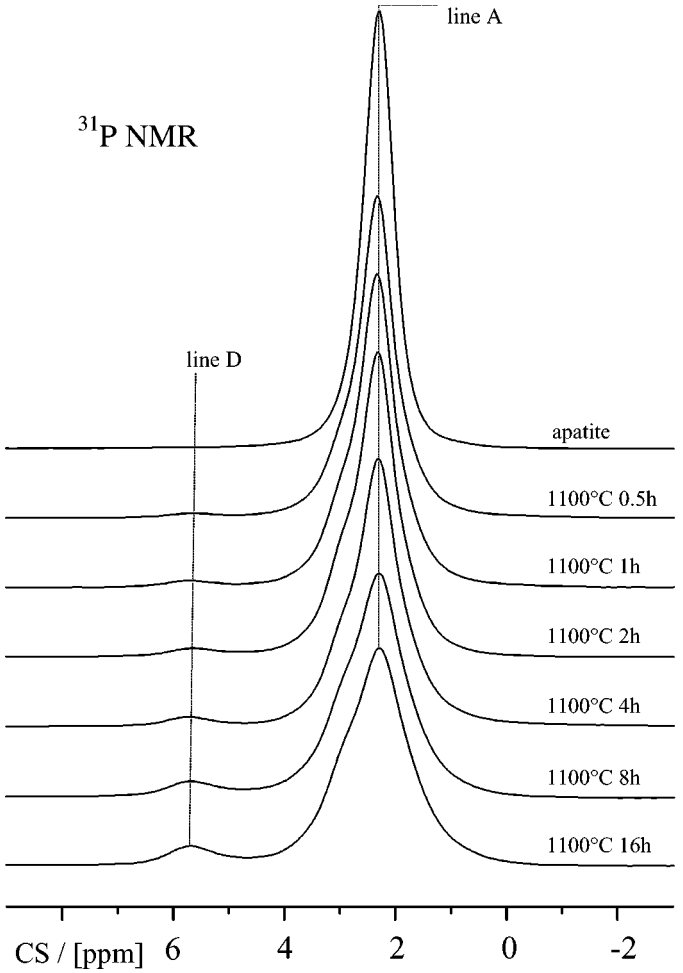

FIG. 6. ^{31}P MAS NMR spectra of the heat-treated hydroxyapatite samples of series A (fixed temperature of 1100°C) compared to the initial crystalline hydroxyapatite (resonance frequency $\nu_0 = 161.92$ MHz, spinning speed $\nu_R/2\pi = 12.5$ kHz, and repetition time $t_{re} = 200$ s).

only slightly. The line width of line D changes little, whereas that of line C increases significantly (at 1150°C). The relative content of the lines C and D remains at all temperatures nearly 2:1 and may be therefore attributed to one type of phosphorus short-range structure. Especially the well-resolved line D (at 5.6 ppm to 5.9 ppm) could be used to monitor the thermal history of a heat-treated apatite sample.

Figure 6 shows the ^{31}P MAS NMR spectra of series A, obtained by heat treatment at fixed 1100°C for different times. The spectra possess the same four lines A–D with comparable chemical shifts and MAS line width. Even for the longest duration heat treatment of 16 h in sample A6 (1100°C/16 h), the NMR parameter and therefore the phosphate short-range structure are comparable to those of sample B4 (1150°C/2 h). To characterize the influence of both temperature and time, a much larger field of parameters needs to be investigated. However, the ^{31}P NMR spectra of series A prove that heat treatment at low temperatures for long times and heat treatment at much higher temperatures but for short times yield the same short-range phosphate structure, supporting the idea that our heat-treated samples are good analogs of plasma-sprayed material.

Figure 7 shows the ^{1}H MAS NMR spectra of series B, and Fig. 8 shows the corresponding line fit analysis of the spectra. Depending on the applied temperature, the spectra possess up to four lines. Line L is attributed to the well-known proton line position of the crystalline hydroxyapatite (see Fig. 1). Much more difficult is the interpretation of

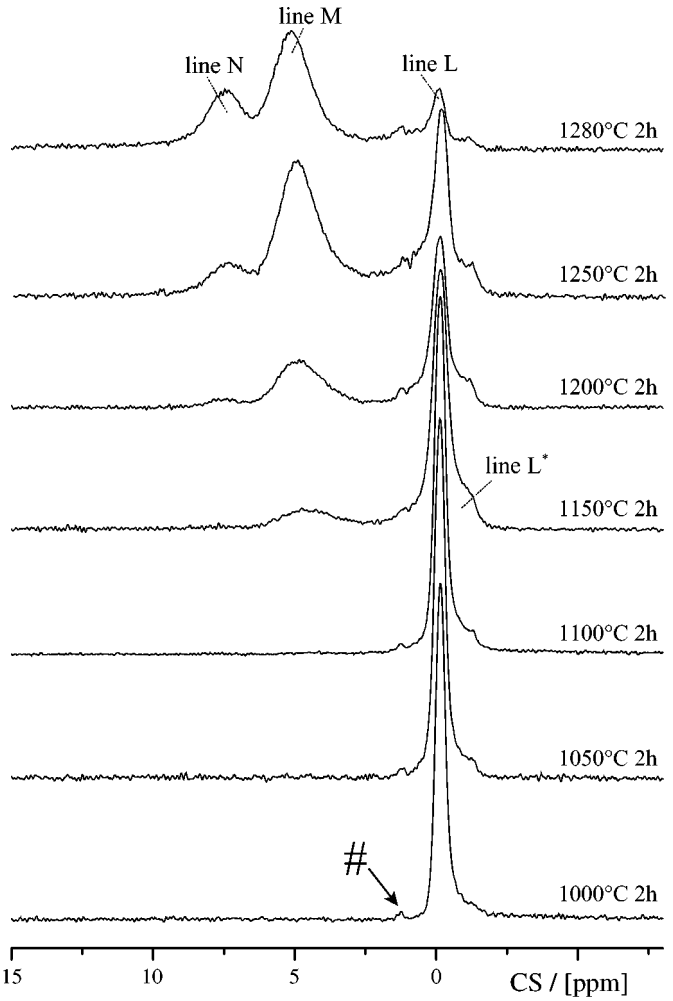

FIG. 7. ^{1}H MAS NMR spectra of the heat-treated hydroxyapatite samples of series B (fixed time of 2 h) compared to the initial crystalline hydroxyapatite (resonance frequency $\nu_0 = 300.2$ MHz, spinning speed $\nu_R/2\pi = 12.5$ kHz, and repetition time $t_{re} = 30$ s). The line marked # is caused by adsorbed water.

the broad line L*. The isotropic chemical shift of the spectral component is close to the original hydroxyapatite position but the line width is about 4 times higher ($\nu_{1/2} = 1.6$ ppm). It could not be excluded that line L* represents several unresolved line positions. However, the averaged isotropic shift line L* could be attributed to protons in distorted hydroxyapatite short-range structures.

Starting at temperatures of 1150°C, the intensity of both proton positions decreases proportionally while two additional lines (M at $\delta_{iso} = 5.2$ ppm and N at $\delta_{iso} = 7.5$ ppm) occur in the ^{1}H spectra. 2D proton double-quantum spectra imply that these peaks arise from OH^- groups which are adjacent to vacancies in the OH^- substructure. It is likely that line M represents those OH^- positions missing only one neighboring OH^- ion, whereas line N is the signal of

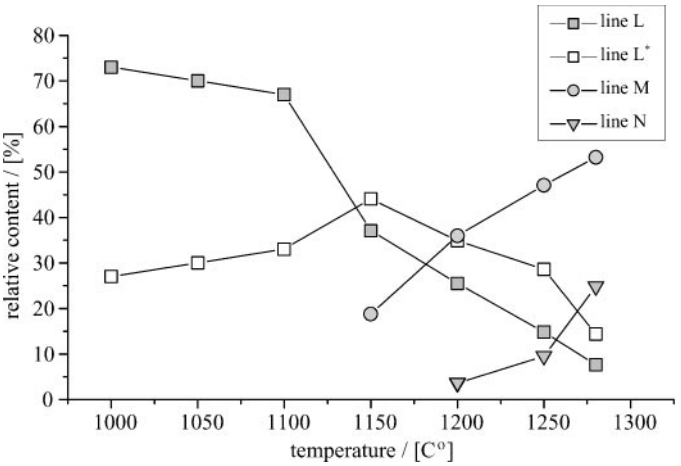

FIG. 8. Relative content of the four different proton positions of the heat-treated hydroxyapatites of series B, obtained by line fit analysis of the ^{1}H NMR spectra.

isolated OH^- groups in the channel. As a typical example, Fig. 9 shows the ^{1}H double-quantum spectrum of sample B6 (1250°C/2 h). In the two-dimensional double-quantum NMR spectra, the peak intensity is proportional to the number and inversely proportional to the distance of

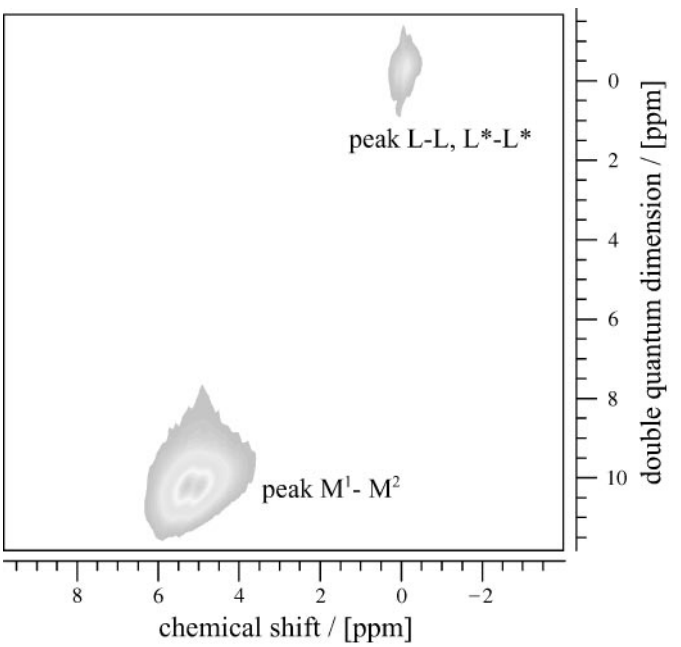

FIG. 9. 2D ^{1}H double-quantum correlation spectrum of heat-treated hydroxyapatite (1250°C/2 h, sample B6). The resonance frequency was $\nu_0 = 300.6$ MHz, spinning frequency $\omega_R/2\pi = 12.5$ kHz, pulse width $t_w = 5$ μs, and repetition time $t_r = 5$ s. The double-quantum excitation and reconversion periods were each 640 μs. The 256×64 data points were collectively rotor-synchronized, by the States method, and with 256 scans per point.

neighboring hydrogen atoms. Double-quantum spectra can be therefore used to investigate the distance of several protons in the structure. The double-quantum spectra of the heat-treated HA possess only two correlation peaks. The peak at -0.1 ppm corresponds to line L and L* in the MAS spectra and is typical for hydroxyapatite structures (even if the short-range structure is slightly distorted). Very surprising is the fine structure of the M peak. In contrast to the one-dimensional MAS spectra, the two-dimensional M peak possesses doublet structure (M^1 at 5.0 ppm and M^2 at 5.4 ppm). The doublet structure of the M peak indicates the existence of isolated pairs of protons in the channel structure of the dehydrated apatites. Depending on the degree of dehydration, residual OH^- groups in the channel structure of the oxyhydroxyapatites ($Ca_{10}(PO_4)_6(OH)_{2-2x}O_x$) possibly form pairs stabilized by a bridging hydrogen bond. In contrast to the proton positions L, L*, and M, the line N (at 7.5 ppm in MAS spectra) gives no double-quantum correlation peak at all. Thus, the N protons are really isolated protons, separated by at least one proton vacancy (more than 3.44 Å (8–10)). Summarizing, 2D double-quantum proton NMR indicate the presence of three different types of OH^- groups along the channels of the apatite structure. Besides the nearly unchanged hydroxyapatite short-range structures (L, L* protons), OH^- pairs (M^1, M^2) and isolated OH^- groups occur. The relative content of that intermediate structure depends on the absolute residual proton content in the sample. To check that all proton positions are located in the oxyhydroxyapatite channel structure and not in a separate phase, the proton positions need to be correlated to the phosphate anion's structure.

To investigate this correlation, 2D ^1H–^{31}P HETCOR NMR spectra have been measured. A typical HETCOR spectrum (sample B7 1280°C/2 h) is shown in Fig. 10a. The spectrum possesses three two-dimensional correlation

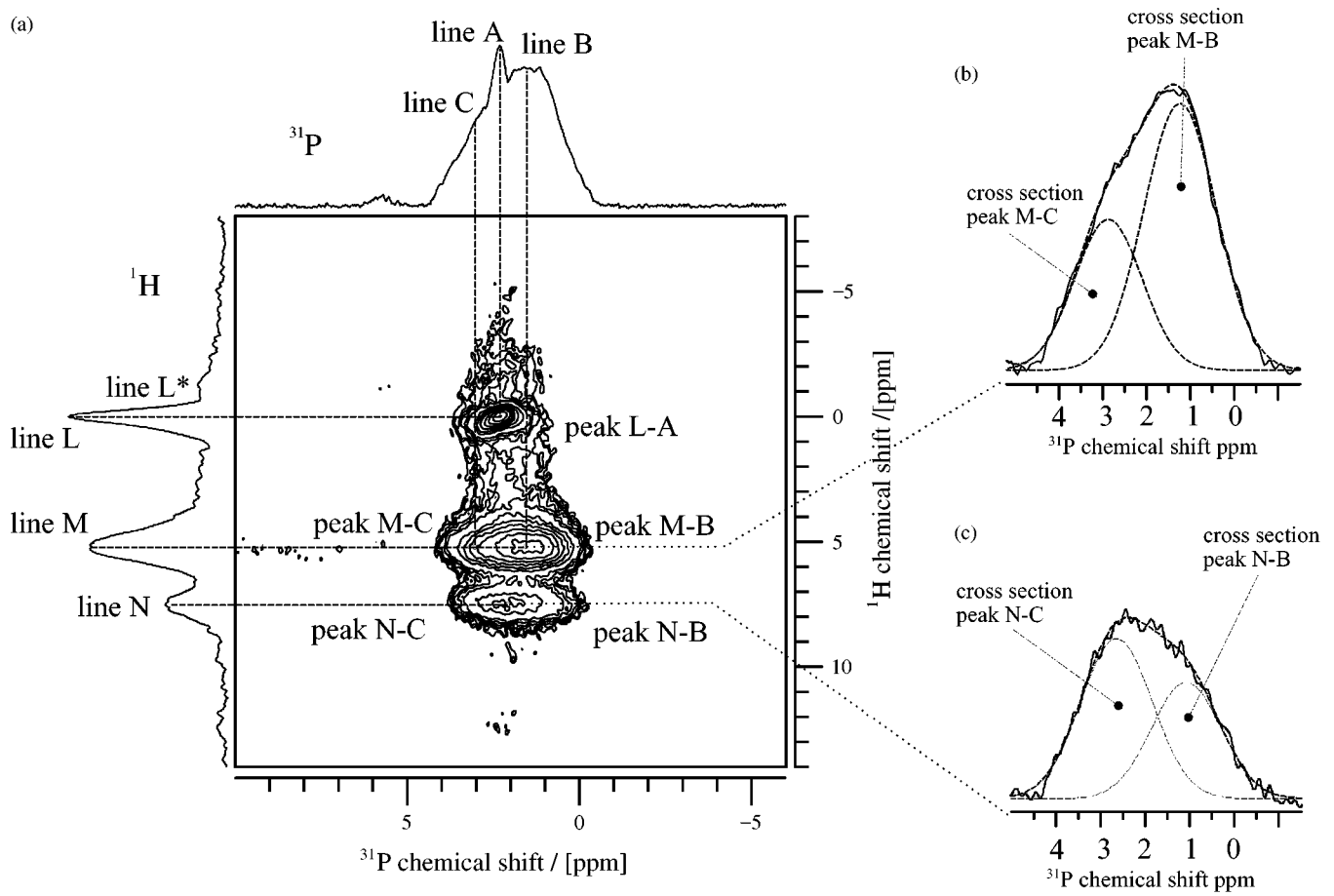

FIG. 10. (a) 2D ^{31}P–^1H HETCOR spectrum of heat-treated (1280°C/2 h, sample B7) hydroxyapatite (spinning speed $\nu_R/2\pi = 12.5$ kHz repetition time $t_{re} = 10$ s and contact time $t_{cp} = 5$ ms). (b) Fitted cross section of the HETCOR spectrum at the proton frequency of line M. The fit analysis proves the doublet nature of the peak M–B, M–C in the ^{31}P dimension. (c) Fitted cross section of the HETCOR spectrum at the proton frequency of line N. The fit analysis proves the doublet nature of the peak N–B, N–C in the ^{31}P dimension.

peaks. It should be noted that the intensity of those two-dimensional peaks is now proportional to the number of involved phosphorus and hydrogen atoms and their reciprocal distance. The sharp peak L–A correlates the phosphorus position A to the proton position L and is therefore unambiguously attributed to an undisturbed hydroxyapatite short-range structure. The broad line L* also correlates to the phosphorus position A. However, the relative intensity of the correlation peak is very low. Very surprising is the absence of B–L or B–L* correlation peaks. Assuming comparable cross polarization efficiency, this fact suggests that line B is associated with large distorted proton-free domains. More difficult is the assignment of the peaks correlating the proton line M to the phosphorus structure (peaks M–B and M–C). It should be noted that the resolution in the HETCOR spectrum is significantly lower than that in the proton double-quantum spectra. Therefore, the proton M doublet was not resolved in the ^{1}H dimension. Figure 10b shows a fitted cross section of the HETCOR spectrum of Fig. 10a at the proton frequency of line M. The fit analyses prove the doublet nature of that peak (M–B and M–C) in the ^{31}P dimension. Thus, both phosphorus positions C and B can be assigned to two distinct phosphorus structure motives in the neighborhood of the OH^- pair ($M^{1,2}$). The fit analysis of the fourth correlation double peak N–B, N–C is shown in Fig. 10c. It correlates the isolated proton (line N) to the phosphorus positions B and C. That result proves the proximity of the isolated proton position to the phosphorus positions B and C. Summarizing the fit analysis of Figs. 10b and 10c, it needs to be considered that the phosphorus atoms B and C are in proximity to both the isolated protons and the proton pairs in the apatite channel structure. The HETCOR spectra possess no correlation peaks of the ^{31}P line D. The very small intensity in this spectral region is obviously caused by long-range contacts without any resolved peaks. The missing D line correlation peaks in the HETCOR spectra prove that line D represents PO_4 tetrahedra in a proton-free region of the apatite channel structure.

There is no reference to phase separation during dehydration. All proton NMR signals are attributed to phosphorus resonances. Any phase separation of the proton-containing structures could therefore be excluded. Vice versa, the phosphorous resonances A, B, and C are attributed to the corresponding proton resonances, and therefore to the oxyhydroxyapatite structure. The only proton-free phosphorus position is line D. However, the phosphorus double-quantum spectra (see Fig. 4) prove that the phosphor tetrahedra represented by line D belong to the oxyhydroxyapatite phase too.

To summarize, the combined application of ^{1}H and ^{31}P NMR spectroscopy including two-dimensional H–H, P–P, and H–P experiments has allowed semiquantitative determination of four different local environments for both H and P, and deduction of some structural characteristics of each environment.

IR Investigations

Figures 11 and 12 show the IR absorbance spectra of the samples B1–B7 in the region of PO_4 fundamental vibrations and the O–H stretching vibration, respectively. The band positions of the initial (not heat-treated) sample is typical for highly crystalline hydroxyapatite (11). The overall intensity of the spectra decreases with increasing temperature. However, the drop in intensity is significantly different for the several band positions. Both the O–H stretching vibration at 3571 cm^{-1} and the O–H libration at 632 cm^{-1} decrease even for temperatures above 1000°C and are almost vanishing at 1280°C. However, the integral intensity of the OH stretching vibration can give only the relative OH^- content (relative to hydroxyapatite). The cause is the poor homogeneity and the estimated thickness (determined relative to the Nujol reference with the assumption of smooth layers) of the Nujol–sample mixtures.

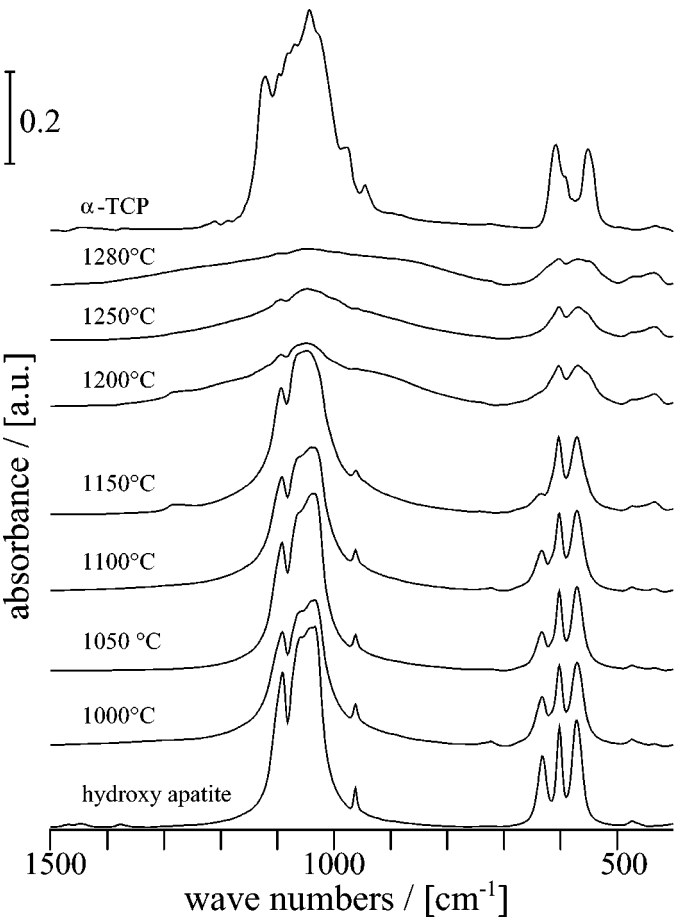

FIG. 11. Scaled IR absorbance spectra of series B (samples B1–B7) compared to that of crystalline hydroxyapatite and α-TCP in the region of the fundamental vibration of PO_4^{3-}.

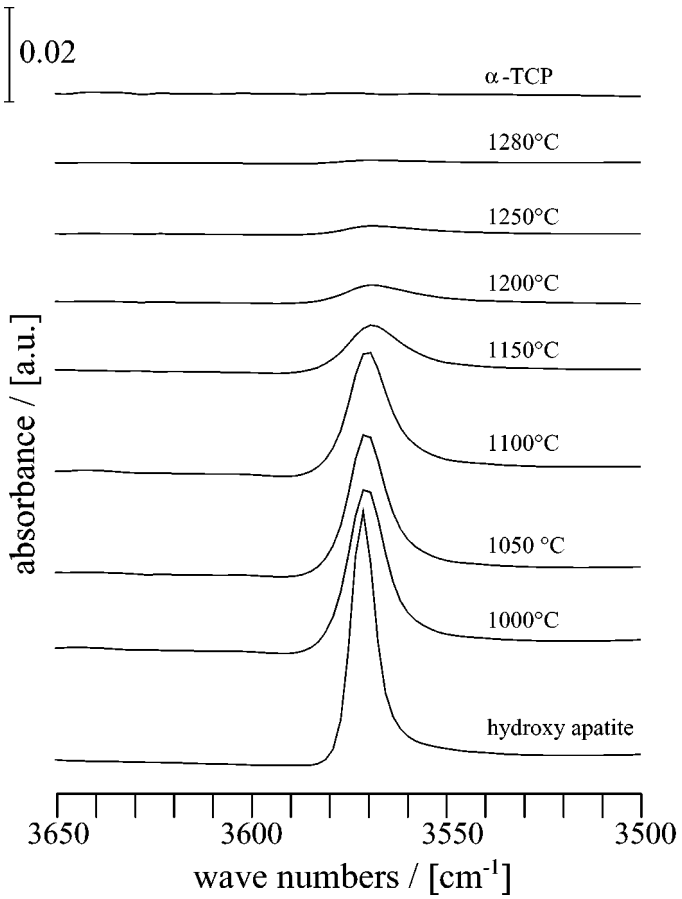

FIG. 12. Scaled IR absorbance spectra of series B compared to that of crystalline hydroxyapatite and α-TCP in the region of the OH stretching vibration.

CONCLUSIONS

The NMR spectra, and hence the deduced local structure, of oxyhydroxyapatites produced by heat treating and plasma spraying of hydroxyapatite are very similar. Thus, the oxyhydroxyapatites are suited as model structures for the variety of plasma-sprayed hydroxyapatites.

The combined application of ^{1}H and ^{31}P NMR experiments has enabled us to study the variety of local phosphorus and proton environments and their evolution with temperature and time. ^{1}H–^{31}P HETCOR has allowed correlation of proton environments with phosphorus environments, allowing us to deduce some aspects of the chemistry of the different domain types.

Four types of phosphorus environments are associated with NMR peaks A–D, respectively. Narrow peak A corresponds to that for untreated hydroxyapatite. Peak B is at a similar chemical shift but broader, suggesting local distortion of the phosphorus environment, but broad peaks C and D are at more positive chemical shift. Four hydrogen environments are implied by peaks L, L*, M, and N. Again, narrow peak L corresponds to that for ideal hydroxyapatite with continuous OH^- groups along the channels of the structure. L* is at similar chemical shift but broader, corresponding to a distorted version of the structure. Two-dimensional data showed that M and N correspond to pairs of OH^- and single OH^-, respectively, bracketed by vacancies in the channels. Cross-correlation ^{1}H–^{31}P HETCOR data imply coexistence of the following local structure types:

1. $A(^{31}P) + L(^{1}H) \rightarrow$ ideal hydroxyapatite
2. $A(^{31}P) + L^*(^{1}H) \rightarrow$ undistorted PO_4 but OH perturbed
3. $B(^{31}P) \rightarrow$ distorted PO_4 with no nearby OH
4. $B(^{31}P) + M,N(^{1}H) \rightarrow$ distorted PO_4 with single and paired OH
5. $C(^{31}P) + M,N(^{1}H) \rightarrow$ strongly distorted PO_4 with single and paired OH
6. $D(^{31}P) \rightarrow$ very strongly distorted PO_4 with no nearby OH.

Types 1–3 predominate for low-temperature runs. Increase of temperature causes progressive increase in domains of types 5 and 6.

ACKNOWLEDGMENTS

The generous support of this work by the Deutsche Forschungsgemeinschaft (Vo-591/2-1 and Vo-591/2-2) is gratefully acknowledged. Furthermore, we thank FRIADENT GmbH for the medically pure hydroxyapatite samples.

REFERENCES

1. W. Lacefield, S. Metsger, N. Blumenthal, P. Dycheyne, J. Davis, J. Kay, J. Stevenson, and R. Salsbury, *J. Appl. Biomater.* **1,** 84 (1990).
2. P. E. Wang and T. K. Chaki, *J. Mater. Sci.: Mater. Med.* **4,** 150 (1993).
3. J. Vogel, P. Hartmann, C. Rüssel, G. Günther, F. Vizethum, and N. Berger, *J. Mater. Sci.: Mater. Med.* **7/8,** 495 (1996).
4. K. A. Gross, V. Gross, and Ch. C. Berndt, *J. Am. Ceram. Soc.* **81**(1), 106 (1998).
5. M. Bohner, J. Lamaitre, A. P. Legrand, J.-B. DÈspinose de la Caillerie, and P. Belgrand, *J. Mater. Sci.: Mater. Med.* **7,** 457 (1996).
6. M. Feike, D. E. Demco, R. Graf, J. Gottwald, S. Hafner, and H. W. Spiess, *J. Magn. Reson. Ser. A* **122,** 214 (1996).
7. A. Pines, M. G. Gibby, and J. S. Waugh, *J. Chem. Phys.* **59,** 569 (1973).
8. M. I. Kay, R. A. Young, and A. S. Posner, *Nature* **204,** 1050 (1964).
9. J. C. Elliott, P. E. Mackie, and R. A. Young, *Science* **180,** 1055 (1973).
10. G. Chi and J. P. Yesinowski, *Chem. Phys. Lett.* **205,** 1 (1993).
11. K. C. Blakeslee and R. A. Condrate, Sr., *J. Am. Ceram. Soc.* **54,** 559 (1971).
12. H. Sfihi, A. P. Legrand, X. Ranz, and C. Rey, *Phosphorus Res. Bull.* **6,** 13 (1996).
13. R. McPherson, N. Gane, and T. J. Bastow, *J. Mater. Sci.: Mater. Med.* **6,** 327 (1995).